

Capturing Nonlinear Electron Dynamics with Fully Characterised Attosecond X-ray Pulses

Lars Funke^{1*†}, Markus Ilchen^{2,4,5*†}, Kristina Dingel^{16,17},
Tommaso Mazza⁴, Terence Mullins^{4,5}, Thorsten Otto⁵,
Daniel E. Rivas⁴, Sara Savio¹, Svitozar Serkez⁴, Peter Walter^{2,12,18},
Niclas Wieland², Lasse Wülfing¹, Sadia Bari^{5,13}, Rebecca Boll⁴,
Markus Braune⁵, Francesca Calegari⁵, Alberto De Fanis⁴,
Winfried Decking⁵, Andreas Duensing⁶, Stefan Düsterer⁵,
Felix Egun⁸, Arno Ehresmann^{3,17}, Benjamin Erk⁵,
Danilo Enoque Ferreira de Lima⁴, Andreas Galler⁴,
Gianluca Geloni⁴, Marc Guetg⁵, Jan Grünert⁴, Patrik Grychtol⁴,
Andreas Hans^{3,17}, Arne Held¹, Ruda Hindriksson¹⁶, Till Jahnke⁹,
Joakim Laksman⁴, Mats Larsson⁷, Jia Liu⁴, Jon P. Marangos⁸,
Lutz Marder^{3,17}, David Meier^{14,17}, Michael Meyer⁴,
Najmeh Mirian⁵, Christian Ott⁹, Christopher Passow⁵,
Thomas Pfeifer⁹, Patrick Rupprecht^{9,10,15}, Albert Schletter⁶,
Philipp Schmidt⁴, Frank Scholz⁵, Simon Schott¹⁶,
Evgeny Schneidmiller⁵, Bernhard Sick^{16,17}, Kai Tiedtke⁵,
Sergey Usenko⁴, Vincent Wanie⁵, Markus Wurzer⁶,
Mikhail Yurkov⁵, Vitali Zhaunerchyk¹¹, Wolfram Helml^{1*}

¹Fakultät Physik, Technische Universität Dortmund,
August-Schmidt-Straße 1, 44227 Dortmund, Germany.

²Institut für Experimentalphysik, Universität Hamburg, Luruper
Chaussee 149, 22761 Hamburg, Germany.

³Institut für Physik und CINSaT, Universität Kassel,
Heinrich-Plett-Straße 40, 34132 Kassel, Germany.

⁴European X-Ray Free-Electron Laser Facility GmbH, Holzkoppel 4,
22869 Schenefeld, Germany.

⁵Deutsches Elektronen-Synchrotron DESY, Notkestr. 85, 22607
Hamburg, Germany.

⁶Physik-Department, TUM School of Natural Sciences, Technische
Universität München, James-Franck-Straße 1, 85748 Garching, Germany.

- ⁷Department of Physics, AlbaNova University Center, Stockholm University, SE-106 91, Stockholm, Sweden.
- ⁸Blackett Laboratory, Imperial College London, London SW7 2AZ, United Kingdom.
- ⁹Max-Planck-Institut für Kernphysik, Saupfercheckweg 1, 69117 Heidelberg, Germany.
- ¹⁰Chemical Sciences Division, Lawrence Berkeley National Laboratory, 1 Cyclotron Road, Berkeley, CA 94720 USA.
- ¹¹Department of Physics, University of Gothenburg, 41296 Gothenburg, Sweden.
- ¹²SLAC National Accelerator Laboratory, 2575 Sand Hill Road, Menlo Park, CA 94025, USA.
- ¹³Zernike Institute for Advanced Materials, University of Groningen, 9747 AG Groningen, The Netherlands.
- ¹⁴Optik und Strahlrohre, Helmholtz-Zentrum Berlin für Materialien und Energie GmbH, Hahn-Meitner-Platz 1, 14109, Berlin, Germany.
- ¹⁵Department of Chemistry, University of California, Berkeley, CA 94720 USA.
- ¹⁶Intelligent Embedded Systems, Universität Kassel, Wilhelmshöher Allee 73, 34121 Kassel, Germany.
- ¹⁷Artificial Intelligence Methods for Experiment Design (AIM-ED), Joint Lab Helmholtzzentrum für Materialien und Energie, Berlin (HZB) and University of Kassel, Berlin, Germany.
- ¹⁸TAU Systems, 201 W 5th Street, Austin, TX 78701, USA.

*Corresponding author(s). E-mail(s): lars.funke@tu-dortmund.de; markus.ilchen@uni-hamburg.de; wolfram.helml@tu-dortmund.de;

†These authors contributed equally to this work.

Abstract

Attosecond X-ray pulses are the key to studying electron dynamics at their natural timescale in specifically targeted electronic states. They promise to build the conceptual bridge between physical and chemical photo-reaction processes. Free-electron lasers (FELs) have demonstrated their capability of generating intense attosecond X-ray pulses. The use of SASE-based FELs for time-resolving experiments and investigations of nonlinear X-ray absorption mechanisms, however, necessitates their full pulse-to-pulse characterisation which remains a cutting-edge challenge. We have characterised X-ray pulses with durations of down to 600 attoseconds and peak powers up to 200 GW at ~ 1 keV photon energy via angular streaking at the Small Quantum Systems instrument of the European XFEL in Germany. As a direct application, we present results of nonlinear X-ray-matter interaction via time-resolved electron spectroscopy on a transient system, observing single- and double-core-hole generation in neon atoms. Using the derived temporal information about each single X-ray pulse, we reveal an otherwise hidden peak-intensity dependence of the probability for formation of double-core vacancies in neon after primary K-shell ionisation. Our results advance the field of attosecond science with highly intense and fully characterised X-ray pulses to the state-specific investigation of electronic motion in non-stationary media.

Introduction

Attosecond physics based on high-harmonic generation (HHG) of optical lasers has been developed from an experimental novelty to a Nobel prize-winning area of fundamental research [1, 2]. It has been extended to measurements of electron tunnelling in atoms [3], timing the photoemission from metal surfaces and bulk material [4] as well as investigating excited states in atoms [5], molecules [6, 7] and in the form of plasmons [8]. Nevertheless, many desirable investigations have been hampered by the limited energy tunability and relatively low flux at higher photon energies in the soft X-ray range achievable with HHG from longer driving laser wavelengths [9, 10]. An alternative approach to generate attosecond X-ray pulses, based on X-ray free-electron lasers (XFELs) [11], holds the promise to overcome these challenges. The highly relativistic electron bunches that produce the intense X-ray pulses via alternating magnetic fields can be shaped in various ways in order to enter the attosecond regime. Over the past decade, significant progress has been made in the compression of FEL pulses spanning the energy range from soft to hard X-rays [12–14]. These advancements have been driven by various methodologies including nonlinear compression [15], fresh slice techniques [16], emittance spoilers [17], and enhanced methods for self-amplification of spontaneous emission (SASE) [18]. Particularly noteworthy are the latest achievements in attosecond pulse generation at FELs, showcasing attosecond pump/probe capabilities [19, 20], as well as the generation of high-power attosecond pulses [21]. The shortening of pulse durations from the femtosecond to the attosecond scale represents a breakthrough in ultrafast FEL science allowing to produce highly intense X-ray pulses precisely tunable in photon energy, and thus to element-specifically address electrons in nonlinearly populated states with strongly increased efficiency [22].

Attosecond X-ray pulses offer efficient access to the exploration of ultrafast processes in transient states such as coherent electron motion in molecules [23], the multielectron effects of post-collision interaction [20], structural configurations after valence ionisation in liquid water [24] and nonlinear X-ray interactions [25, 26]. Most importantly, the single-shot temporal characterisation of SASE FEL pulses is a prerequisite for the accurate interpretation of all sorts of experimental results, e.g. from high-intensity coherent X-ray diffraction and imaging measurements [27, 28]. Thus, the creation and exploration of transient states of matter with high-power attosecond X-ray pulses requires the full knowledge about the temporal characteristics of individual FEL pulses [18, 19, 29]. This is not merely an incremental step towards advanced time and spatial resolution, but rather the opening to a new scientific field between physics and chemistry, with rich opportunities for understanding nature’s dynamics literally at their core.

However, the underlying stochastic nature of the XFEL pulse generation by self-amplification of spontaneous emission [30] used by most of the existing FEL photon sources limits the possible control of the X-ray pulses’ time–energy structure. Despite several attempts to predict pulse characteristics using standard accelerator and photon diagnostics alongside machine learning (ML) approaches [31–33], accurate delivery of the time and energy structure especially with highly manipulated bunches for the production of attosecond pulses remains elusive. High-repetition-rate SASE XFELs

[34] can mitigate this limitation by covering a broad pulse structure distribution, combined with a non-invasive pulse-by-pulse diagnostics and near-online spectro-temporal analysis method based on 'angular streaking' [19, 35, 36]. In this scheme, illustrated in Figure 1 and explained in more detail in the next section, the total set of stochastic pulse shapes can be sorted by an evaluation algorithm for suitable temporal structures. In recent experiments, angular streaking was already used to determine an overall regime of attosecond pulse durations for specific FEL operation modes, without using the varying single-shot X-ray pulse structure as a parameter for further physical analyses [20, 23, 24].

Here, we report on the generation and characterisation of isolated pulses of up to 200 GW peak power at 990 eV photon energy and a duration as low as $\sim 700 \pm 270$ as at the SASE-based European XFEL. We present systematically varying pulse-duration distributions for two different operation modes, as well as time-delayed pump/probe sequences of double-peak attosecond pulses with various delays and spectral compositions. For the characterisation of the single-shot angular streaking data, we utilised a well-established iterative approach [19] as well as a recently developed machine-learning technique [37], which allows for similar reconstruction quality using less computation time and bearing the potential for online pulse characterisation. Due to the high intensity of the XFEL pulses, ionic or excited states of matter can be created efficiently [38–43], and the emerging dynamics can be interrogated via the very same pulse with fully determined characteristics. We show this capability by simultaneously measuring attosecond X-ray pulse shapes and the duration-dependent formation of double-core-hole states in gaseous neon. Thus, we combine attosecond single-shot photoelectron spectroscopy of extremely short-lived transient species with resonant X-ray excitation, paving the way for further time-resolved studies of more complex quantum systems, e.g. organic and/or chiral molecules, where coupled electronic and nuclear dynamics can be disentangled.

To generate attosecond SASE pulses at the European XFEL, we used a combination of increasing the FEL gain and reducing the length of the lasing window of the electron bunches in the accelerator. We achieved this with the chirp-dispersion method [44], using a non-standard approach for controlling the dispersion, with the additional benefit of increasing the peak current. A more detailed description of this attosecond pulse generation mechanism can be found in the Supplementary Information (SI) and will be also presented elsewhere.

SASE pulse characterisation

The temporal characteristics of the pulses can usually only be inferred indirectly in the SQS branch of the beamline from destructive, i.e. photon-absorbing, measurements of the X-ray pulse spectra via a grating spectrometer [45] or indirect methods such as cross-correlation measurements [46, 47], the latter providing only average pulse durations.

We employ angular streaking, the only currently available direct and non-invasive method for characterizing the temporal and spectral X-ray structures of single FEL pulses, i.e. the number of SASE peaks (and their sub-femtosecond durations), as

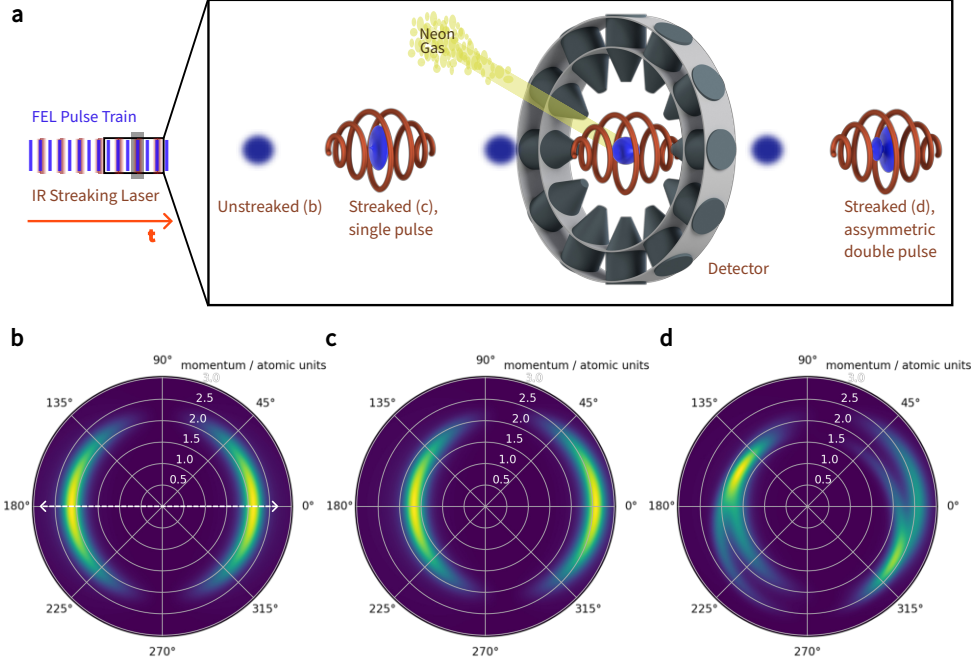


Fig. 1 a) Schematic overview of the angular streaking experiment. Every other in a train of XFEL pulses is overlapped with circularly polarised mid-infrared streaking laser pulses. The resulting phase-dependent electron energy shift is measured in a time-of-flight photoelectron spectrometer array. **b)–d)** Three examples of simulated neon 1s-electron spectra in the polarisation plane, **b)** an unstreaked shot (no momentum shift), **c)** a short (with respect to the optical cycle of the streaking laser) linearly polarised single FEL pulse: the momentum distribution is shifted to the right, when the vector potential of the streaking laser at the time of interaction points to the right, **d)** a double-peak FEL pulse with a small time delay between the two intensity peaks. The latter demonstrates best the capabilities of the method, as two rings appear in the angle-dependent photoelectron spectrum. With a suitable reconstruction algorithm, arbitrary XFEL pulse shapes can be reconstructed. The dashed white arrow in **b)** indicates the X-ray polarisation, which imposes the angular distribution on the photoelectron emission from the spherically symmetric neon 1s-shell (here simulated in dipole approximation).

well as the spectral chirp for each single shot. This knowledge can be used to find optimised FEL settings for targeted X-ray pulse characteristics, such as the shortest possible pulses, double-peak pulses with defined delay, or two-colour operation modes, as, for example, demonstrated in [48]. The streaking technique in a low-density gas target exerts a negligible influence on the X-rays, with an absorption fraction on the sub-percent level. Consequently, these same pulses can be used in a subsequent experiment, which can now capitalise on the fully determined X-ray characteristics via pulse tagging.

In this scheme, as illustrated in Figure 1, a circularly polarised mid-infrared (MIR) laser pulse is temporally and spatially overlapped with the X-ray FEL pulse in a region filled with neon gas at a partial pressure of approximately 10^{-7} hPa. 1s-electrons

of the neon atoms are ionised by the linearly polarised XFEL pulse. The outgoing photoelectrons interact with the circularly polarised 4.75 μm -wavelength strong-field streaking pulse, changing their momentum and leading to an energy and angular redistribution of the electrons depending on the electric field amplitude and phase of the laser during the window of temporal overlap between X-ray and MIR pulses. The resulting angular and spectral distribution is detected by an array of 16 electron time-of-flight (eTOF) spectrometers, positioned in a plane perpendicular to the joint propagation direction of the MIR laser beam and the FEL around the interaction point [19].

At an FEL photon energy of 990 eV, neon 1s-photoelectrons are emitted with a kinetic energy of approximately 120 eV upon ionisation [49]. Applying suitable electrostatic fields in the flight section of individual spectrometers, we attain about 0.5 eV of energy resolution for the photoelectrons of interest. This enables a robust reconstruction of the X-ray pulse shape using the angular streaking approach. It is noteworthy that this energy-resolution recovery even works for very fast electrons of several hundreds of eV kinetic energy, as detailed below regarding the Auger spectra of neon. The maximum energy shift of the neon 1s photoelectrons induced by the streaking laser is on the order of 15 eV under the given conditions. The spectral and temporal characteristics of individual pulses have been reconstructed using a post-experiment iterative retrieval code similar to the one published by Hartmann et al. [19].

Iterative pulse reconstruction

In this algorithm, a simple semi-classical streaking simulation is performed for ionisation events from single-peak “elementary” FEL pulses, yielding corresponding angle-resolved electron spectra as measured by the circular array of eTOF spectrometers. A time–energy grid of elementary pulses is scanned over a range of streaking phases and FEL photon energies similar to the experiment, generating a so-called basis. Each experimental measurement is considered equivalent to a linear combination of specific basis entries. The goal of the reconstruction is to find the linear combination that produces a retrieval as close as possible to the measurement. This vector is then identified as a “spectrogram”, i.e. a spectro-temporal representation of the SASE FEL pulse (see Figure 2). An iterative algorithm is used to solve this inverse problem: In each iteration, the measured angle-resolved electron spectra (“detector images”) for a single FEL shot are compared to all simulated elementary pulses. The best-fitting one is subtracted incoherently from the data, and energy is added to the resulting spectrogram at the point in time and photon energy corresponding to that entry. This process is repeated until only noise remains, resulting in a complete spectrogram. Further details can be found in Section S2.1 in the Supplementary Information.

Machine-learning-based algorithm for online feedback

For faster and more efficient online-feedback during future experiments, we are currently establishing an ML-based evaluation pipeline. This might be implemented into

the data read-out stream of SASE beamlines, ultimately running simultaneously during the measurement and providing single-shot X-ray pulse information at the full XFEL repetition rate.

The main limitation of the iterative pulse reconstruction algorithm is the analysis speed, which currently does not allow for real-time feedback. The potential for using ML-based ultrafast diagnostic tools is vast. Li et al. [32] linked XFEL electron and photon beam properties to create an ML-based diagnostic tool; Alaa El-Din et al. [33] used ML to predict attosecond two-colour pulses; Brunner et al. [50] utilised ML to map from streaking traces to near-infrared pulses and electron wavepackets; Meng et al. [51] applied ML to learn the mapping from photon spectrograms to attosecond pulses using the all-optical method. In a recent article [37], we have shown that ML, particularly convolutional neural networks, in conjunction with angular streaking holds the potential for online XFEL pulse characterisation and, therefore, online diagnostics.

We used our measurement as a test for the future implementation of such an ML-based method that paves the way for online pulse-reconstructions during experimental campaigns. We here demonstrate that it matches the quality of the iterative pulse reconstruction approach while only taking a fraction of its computation time (cf. Sec. S2.2.1 in the SI). For this, we derived the desired pulse characteristics, such as the XFEL temporal pulse structure, from the detector images using the iterative reconstruction algorithm to generate labels from real-world experimental data, which we used for training the models in a supervised manner. A key challenge for model training is the limitation of labelled experimental data. We opted for a train-validation data split of 90%–10%, resulting in 64776 samples for training and 7200 samples for validation. Additionally, we held back 400 samples which we used for comparing the ML method against the iterative pulse reconstruction algorithm. Figure 3 shows four of the 400 test samples. By utilizing a dropout-based uncertainty modelling technique [52], we can ensure validity of the model’s prediction, which, in addition to further details on the ML pipeline, is described in Sec. S3.2 of the SI. The ML predictions resemble the results of the iterative algorithm. The combination of angular streaking and ML evaluation, as shown here, is the first step towards closed-loop experimentation at XFELs [53].

Intense Attosecond X-ray Pulses

We identified isolated attosecond X-ray pulses ($h\nu = 990$ eV) with a peak power of up to 200 GW, characterised directly with a time-domain measurement on a single-shot basis. Approximately 38% of the shots were found to be shorter than 1 fs in this data set, and approx. 17% below 750 as, with the shortest pulses in the order of 600 as (FEL Setting A in Figure 4). The nonlinear electron-bunch-compression settings were later relaxed to produce slightly longer pulses for comparison (FEL Setting B in Figure 4). As explained above, the stochastic nature of the SASE process leads to very different X-ray pulse shapes, including single-peak attosecond pulses, double-peak structures with variable delays and various forms of more complicated intensity profiles consisting of three or more peaks. To define a common and reproducible measure for the pulse shapes described in this work, all durations are given in terms of the temporal distance

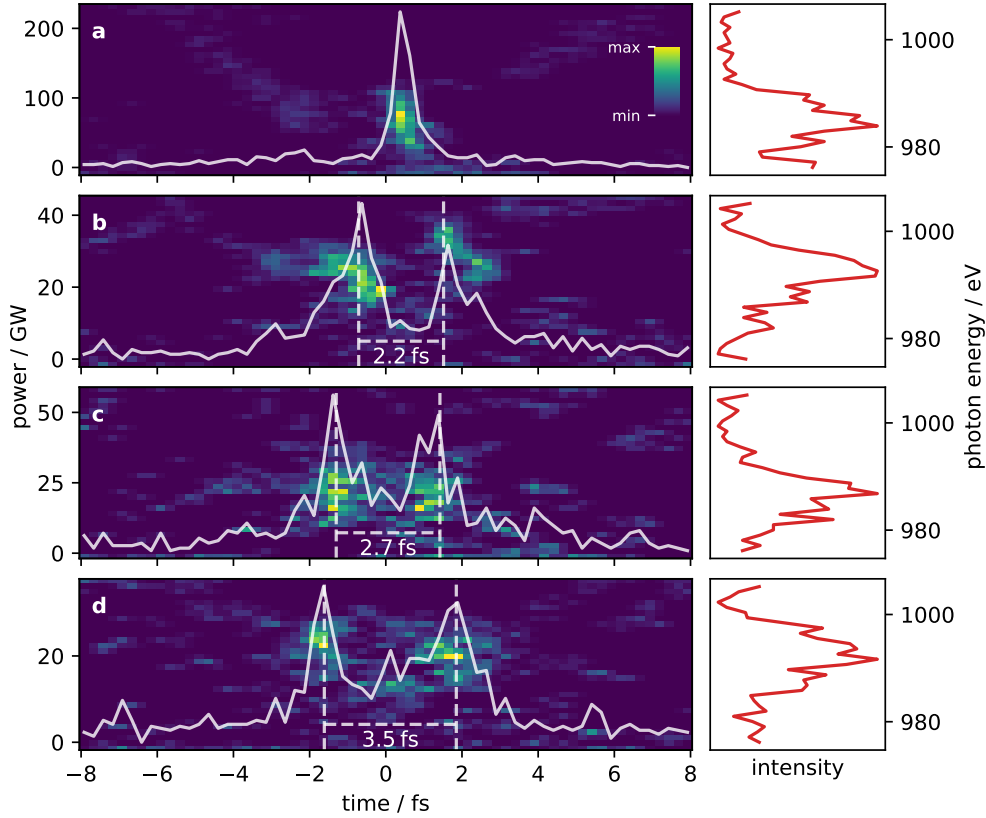


Fig. 2 Examples of reconstructed attosecond FEL pulses. The colour-coded background represents the reconstructed spectrograms (full spectro-temporal information). Overlaid, the temporal shape of the FEL pulses is shown in white. The latter is normalised to the pulse energy to obtain an absolute power figure. The pulse energy is measured independently by the SQS X-ray gas monitor (XGMD). The right panels show the spectrograms' projection onto the spectral axis in red, representing an X-ray photon energy spectrum. **a)** Single-peak 600 attosecond FWHM FEL pulse, **b)–d)** double-peak pulses with varying pulse separation.

between the first and last points, either within a single peak or in a multiple-peak shots, where the temporal power profile reaches a value of half of the maximum (full width at half maximum / FWHM). An example of how this applies to a multi-peak shot is shown in the right-hand inset of [Figure 4](#).

Furthermore, in order to demonstrate the time-resolving capabilities, double-peak attosecond pulses, both at $h\nu = 990$ eV, with individual single-peak powers close to 50 GW have been identified ([Figure 2](#)). Knowledge about the pulse structure allows sorting on peak power as well as applying further analysis methods such as stochastic delay scans. As the European XFEL can deliver >1000 shots per second, this 'post-sorting' yields the promise to get access to X-ray pump/X-ray probe methodology with highly intense pulses and attosecond time resolution without the need of additional infrastructure, like split-and-delay beamlines. [Figure 2 b\)–d\)](#) illustrates

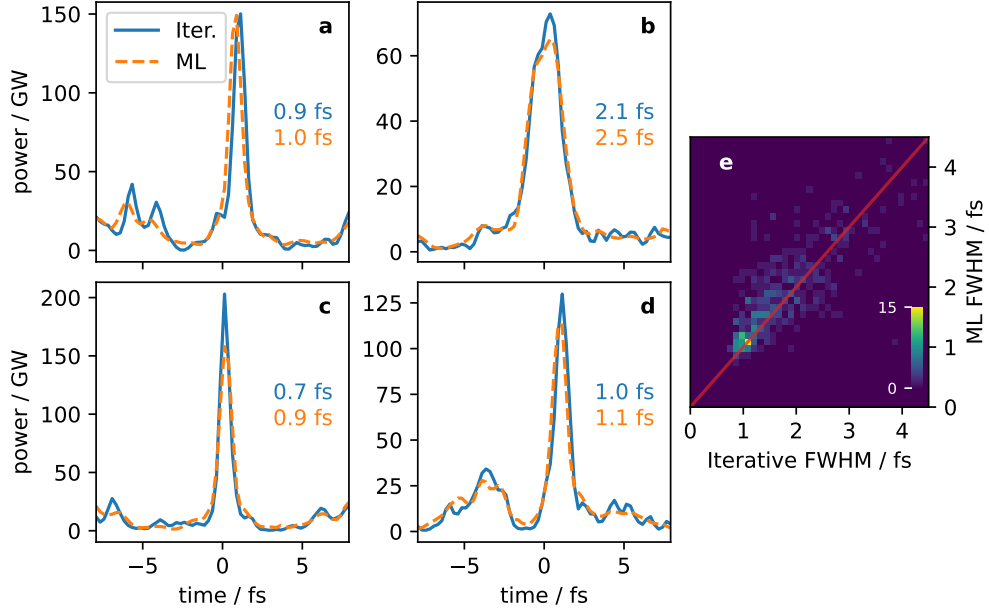


Fig. 3 a)–d) Ultrashort FEL pulse temporal structures derived from the iterative (solid blue line) and ML (dashed orange) reconstruction. The absolute power scale is calculated by normalizing the pulse shape to the total pulse energy. The latter is measured independently by the SQS X-ray gas monitor (XGMD). The indicated durations are the FWHM of the iterative (upper, blue) and ML (lower, orange) reconstructions, respectively. e) Correlation histogram of derived FWHM durations for both methods over all 400 evaluated shots, with the red line indicating a 1:1 correlation. The Pearson correlation coefficient for this data set is 0.91. The slightly longer pulse durations for the ML predictions can be attributed to the tendency of the networks to smoothen over very fine details of the structure, while very closely retaining the pulse shape itself.

exemplary pulse structures in this regard. Together with the high photon energy from the EuXFEL, these pulses have the required intensities, for example, to ultimately enable time-resolved insights into ultrafast *nonlinear* electronic processes as described in the next section.

Attosecond spectroscopy of transient states in neon

In the following, we use the attosecond temporal information about individual SASE pulses in a simultaneous measurement of an X-ray triggered process, leading to a better understanding of the ensuing nonlinear reaction dynamics. We sort individual X-ray shots according to their temporal FWHM, revealing a clear peak-power dependence of the relaxation pathway in highly excited neon ions. For this, we used the adaptability of our detector array and the flexibility of the iterative retrieval code, and tuned separate TOF detectors in the spectrometer setup to two different observation regions with respect to well-resolved electron energies: 12 detectors are kept at the previously mentioned energy at around 120 eV, given by direct photoionisation from the neon 1s shell by a 990 eV X-ray pulse, which is used for the pulse reconstruction. Four

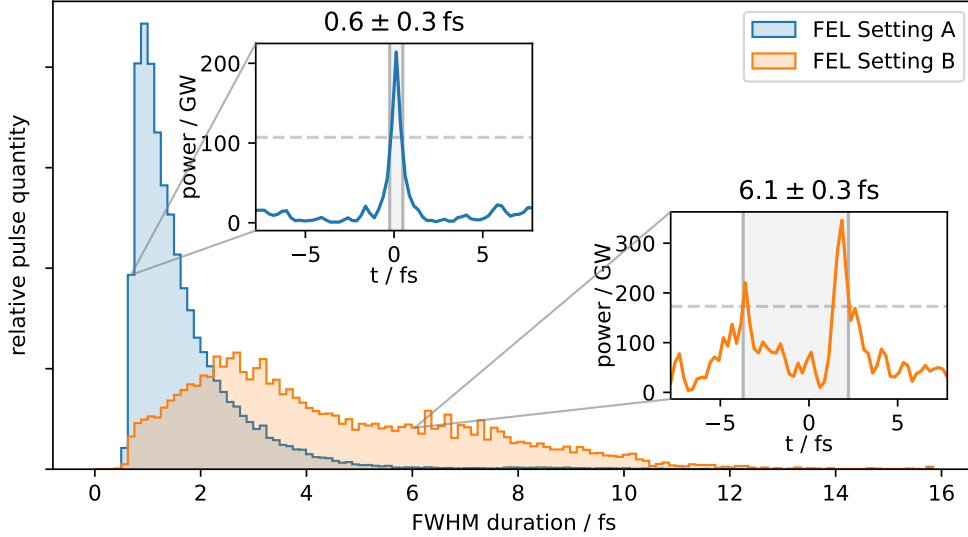


Fig. 4 Distribution of pulse FWHM duration for two evaluated machine operation modes, tuned for shortest possible pulses (Setting A, 72376 shots) and longer pulses (Setting B, 11440 shots). Insets: Exemplary single pulse temporal shapes from the respective data sets with indicated FWHM measurements.

TOF detectors are tuned to resolve much higher kinetic electron energies, mainly between 760 eV and 920 eV, stemming from various Auger processes in the sample after illumination with intense X-ray pulses. The X-ray bandwidth, as determined from our measurement, is approximately 9.4 eV (FWHM).

For a broad variety of relatively light elements with atomic numbers $Z < 30$, the Auger decay after K-shell ionisation or excitation is the predominant relaxation mechanism, occurring typically within a few femtoseconds. Studying core-ionised systems *before* the energy is transferred to the secondary Auger electron, promises insights into the localised non-equilibrium Coulombic environment of a transient state, preceding and thus governing any kind of X-ray-induced dynamics including subsequent structural changes in more complex molecules.

As shown in earlier studies of gaseous atomic neon, highly intense pulses of XFELs allow for sequential double photoionisation, where a core-ionised state is created by a first photon and this short-lived intermediate state is further core-ionised or core-excited by a second photon [39]. In the photon picture, for such a process to occur, it is necessary that the absorption of the second photon precede the Auger decay of the single-core-hole state, which has a lifetime of 2.4 fs [54]. This second photon's energy needs to exceed a significantly increased binding energy for the remaining K-shell electron in the transient neon $1s^{-1}$ system, which amounts to ~ 990 eV [42]. In this case, the core shell of the atom is left empty, and the overall vacancy is termed a double-core hole (DCH). Even more complex dynamics emerge via the multitude of

available DCH Auger decay channels if the second K-shell electron is not promoted to the continuum, but excited into one of the Rydberg states of the transient system [55].

In panel **Figure 5 a)** we show electron spectra of different Auger decay channels in neon, from both, single-core-hole (SCH) and double-core-hole states, with the MIR streaking laser turned on (coloured lines) or off (dashed blue line). The coloured lines represent measurements of the streaked Auger signals, which were taken simultaneously with the X-ray pulse reconstruction spectra from the streaked neon 1s-electron photolines. To best preserve the energy resolution of the main DCH contributions, we filter on a streaking phase such that the spectra are maximally shifted to higher energies, allowing to minimise the effect of spectral broadening of the Auger peaks by the streaking laser field. The line colour indicates subsequently lower pulse durations of the X-ray pulses, decreasing from yellow to black. The total FEL pulse energy is restricted to a narrow window of $200 \mu\text{J} \pm 30 \mu\text{J}$, keeping the total number of photons approximately constant. This corresponds to an intensity on the order of 10^{18} W/cm^2 at the given focal spot size of below $5 \mu\text{m}$. Our results demonstrate the clear pulse-duration and thus peak-power dependence of the nonlinear DCH signal increase [14, 56], under otherwise unchanged FEL conditions (more details on relative pulse energy stability in the SI, especially Fig. S6).

Investigating this dependence further, we integrate the SCH and DCH peak signals within the green and blue shaded areas, which results in the signal yields plotted as circular and triangular symbols in panel **b)**. Both experimental data sets are compared to simulation results (crosses; dotted green for SCH, dash-dotted blue for DCH), based on an approach of solving a set of coupled rate equations using calculated atomic cross sections and Auger-decay lifetimes [57, 58]. Details about the employed theoretical methods and the rate-equation calculations can be found in the SI.

Several considerations need to be taken into account for the interpretation of the displayed FWHM dependence of the DCH and SCH signals. Under the given conditions, in the first step for DCH generation, neon atoms are singly core-ionised by the X-ray pulse. The amount of SCH Auger electrons will predominantly be determined by the total number of X-ray photons, i.e. the signal from single-photon-absorption processes scales linearly with the pulse energy and is independent of the FEL pulse duration. As mentioned above, for the data shown in **Figure 5 b)** we kept the pulse energy and thus the number of photons practically constant, leaving the number of initially generated SCH states unchanged. Since the next step for creating a DCH requires a second photon *in direct sequence before the Auger relaxation can happen*, reducing the pulse duration, and thus increasing the *peak* power, in turn increases the DCH yield by enhancing the probability for further ionising the core-ionised neon atoms. That also implicates for every electron detected after promotion of the singly-ionised neon atom to the DCH state, the respective SCH decay channel is closed. Therefore, we expect a counter-acting decline of the SCH electrons in step with the signal increase due to the nonlinear DCH process.

The DCH and SCH signals presented in panel **b)** show the expected increase of DCH signal with decreasing FWHM [14] of the reconstructed intensity profiles, and thus a direct dependence on the peak power of single X-ray shots. This highlights the ability to employ attosecond-scale knowledge about individual SASE XFEL pulses to

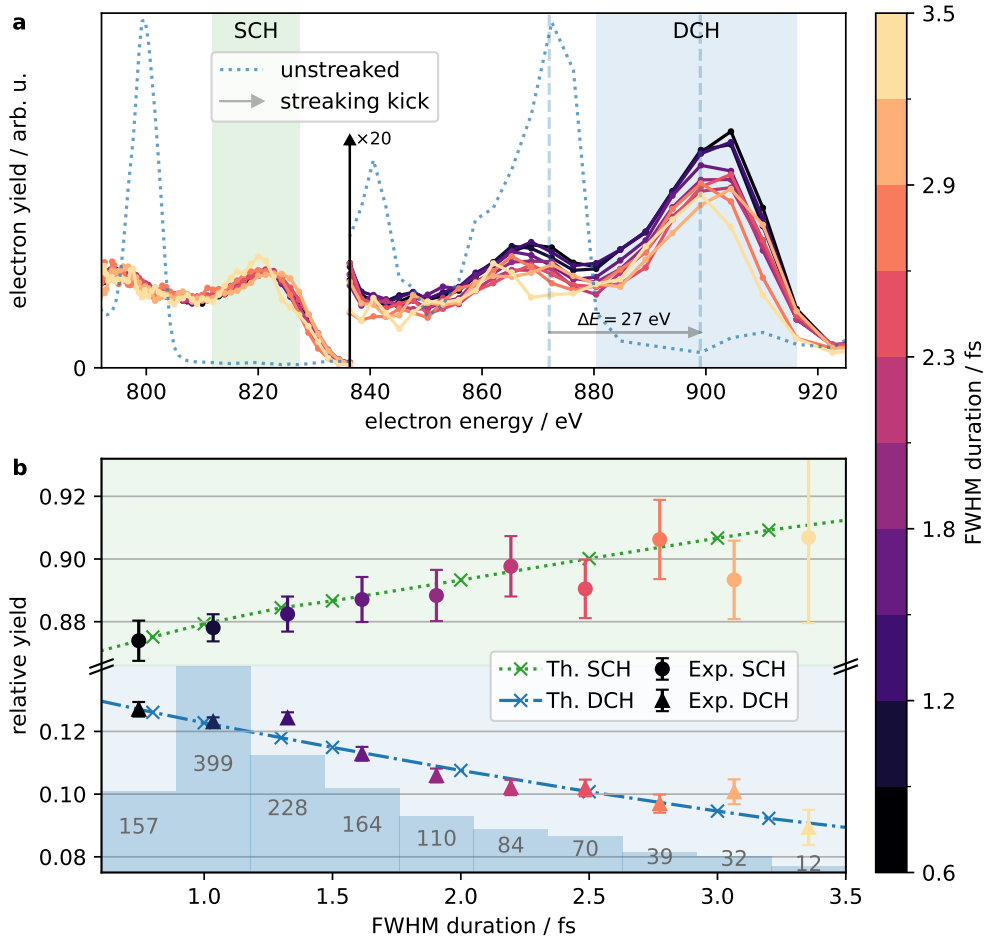


Fig. 5 **a**) Electron spectra of neon irradiated with intense 990 eV FEL pulses, with the MIR laser off (“unstreaked”), averaged over 16018 shots (light-blue dotted line). The $KL_{2,3}L_{2,3}$ single-core-hole Auger line (SCH) is visible at an energy around 800 eV, followed by resonant and non-resonant double-core-hole Auger peaks (DCH) between 870 eV and 880 eV (signal enlarged 20 times for better visibility). The colour-coded lines show averaged electron spectra with the MIR laser on (“streaked”), filtered for a specific streaking laser phase and sorted by pulse duration. Furthermore, only shots within a narrow pulse energy window of 200 ± 30 μ J are selected. The grey arrow indicates the energy shift induced by the MIR field, when compared to the spectrum without streaking laser. **b**) The spectrum in **a**) is integrated over the light-green and light-blue shaded areas to produce a relative yield curve as a function of pulse duration (circles, triangles) for the SCH and DCH peaks. A theoretical model for both yields based on rate equations is shown as green dotted (SCH) and blue dash-dotted (DCH) lines. The experimental data points are normalised such that the lowest-duration point in each series lies on the theory curve. The blue bars with inscribed numbers in the lower half show the number of spectra averaged to yield each respective data point.

uncover intricate details of time-dependent nonlinear effects, based on the measurement of shot-to-shot X-ray pulse shape variations within a single FEL operation mode. These combined measurements not only uncover the nonlinear dependency between X-ray pulse duration and DCH generation probability, but further verify the attosecond X-ray pulse shape reconstruction due to its direct correlation with the DCH dynamics.

In our measurement, we focus on a range of X-ray pulse durations in close vicinity to the expected Auger decay time around 2.4 fs for the SCH state in neon. Locally, the dependence of the DCH signal yield on X-ray duration can be well-fitted by a linear response curve, which only shows its exponential decay characteristics over a broader interval of pulse-duration values (see Fig. S8 in the SI). Higher-order effects due to saturation [39, 59] or additional ionisation of valence electrons and subsequent shifts in excitation energies are mostly beyond the scope of the current study and require more sophisticated simulations based on full quantum-mechanical descriptions. Further investigations of specific reaction pathways and their impact on the timescale of electron dynamics and on the lifetime of excited electronic states will be conducted in the future in order to answer such questions quantitatively. Beyond that, the specific influence of the SASE pulse structure, as accessible by our simultaneous angular streaking X-ray pulse characterisation, instead of the here-demonstrated sorting by FWHM duration, is a very interesting and timely topic for XFEL research.

Summary and Outlook

Enabled by the high intensity of the employed attosecond pulses at 990 eV, we have shown new paths to nonlinear spectroscopy of highly transient states of matter with X-rays. The state-specific exploration of nonlinear electron dynamics via coherent attosecond X-ray pulses is a promising perspective towards exploring the physical origins of reaction processes together with the subsequent chemical evolution and ultimately a system’s functionality. Here, we have demonstrated the generation and measurement of isolated attosecond pulses of up to 200 GW peak power with durations of only about 700 as, opening up the potential for high-repetition rate XFELs to enable studies of nonlinear phenomena in transient media. We were also able to show that ML can keep up with conventional algorithms in terms of pulse reconstruction quality and that ML-usage holds the key to provide online feedback regarding the pulse shapes. While angular streaking allows for studying details of electronic motion and redistribution, it can also readily map out their translation into nuclear dynamics. This method may be used in the future to directly follow electron rearrangement after excitation of specific elements in complex molecules, with the goal to sense and control the electronic evolution in the origins of chemistry with atomic precision and to understand radiation damage mechanisms on a more fundamental level. Intriguing prospects of tracking electron migration in larger molecules such as peptides and amino acids and understanding the mechanisms of functionality-altering energy deposition and subsequent molecular restructuring are opened up. Combining the presented modes with the future possibilities of X-ray polarisation control at FELs will even allow studying the time-dependent asymmetric structures of such systems and their chiral dynamics.

Acknowledgements. We thank European XFEL for provision of beamtime under proposal number #2828 and the many support groups for their sedulous effort. We also thank the DESY photon-science workshop under the lead of Markus Kowalski for their kind and competent help. We thank Elena V. Gryzlova for providing calculations of photoionisation cross sections for the rate equation model. We furthermore thank Raimund Kammering, serving as the run coordinator and providing invaluable support to our activities in the XFEL control room during our experiment. This work has been supported by the Bundesministerium für Bildung und Forschung (BMBF) grant 13K22CHA. M.I., A.E., A.Ha., L.M. acknowledge support from the Deutsche Forschungsgemeinschaft (DFG)-Project No. 328961117-SFB 1319 ELCH (Extreme light for sensing and driving molecular chirality). M.I. acknowledges funding from the Volkswagen Foundation for a Peter-Paul-Ewald Fellowship. L.F., K.D., A.E., A.Ha., A.He., R.H., L.M., D.M., S.S., B.S., L.W., M.I. and W.H. acknowledge funding of the BMBF-ErUM-Pro project “TRANSALP” (05K22PE3) and the BMBF project “SpeAR_XFEL” (05K19PE1). J.P.M. and E.E. acknowledge funding from EPSRC/UKRI EP/X026094/1 and UK Physical Sciences XFEL Hub. This work is supported by the Cluster of Excellence ‘CUI: Advanced Imaging of Matter’ of the Deutsche Forschungsgemeinschaft (DFG) – EXC 2056 – project ID 390715994. P.R. acknowledges funding from the Alexander von Humboldt Foundation (Feodor Lynen Fellowship). M.L., and V.Z. thank the support from the Swedish Research Council (VR) through the Röntgen-Ångström Cluster program (grant No. 2021-05967). S.B. acknowledges funding from the Helmholtz Initiative and Networking Fund. P.R. and T.P. acknowledge support by the Deutsche Forschungsgemeinschaft (DFG, German Research Foundation) under Germany’s Excellence Strategy EXC2181/1-390900948 (the Heidelberg STRUCTURES Excellence Cluster). Data recorded for the experiment at the European XFEL are available at doi:[10.22003/XFEL.EU-DATA-002828-00](https://doi.org/10.22003/XFEL.EU-DATA-002828-00).

References

- [1] Paul, P. M. *et al.* Observation of a Train of Attosecond Pulses from High Harmonic Generation. *Science* **292**, 1689–1692 (2001).
- [2] Hentschel, M. *et al.* Attosecond metrology. *Nature* **414**, 509–513 (2001).
- [3] Uiberacker, M. *et al.* Attosecond real-time observation of electron tunnelling in atoms. *Nature* **446**, 627–632 (2007).
- [4] Cavalieri, A. L. *et al.* Attosecond spectroscopy in condensed matter. *Nature* **449**, 1029–1032 (2007).
- [5] Goulielmakis, E. *et al.* Real-time observation of valence electron motion. *Nature* **466**, 739–43 (2010).
- [6] Sansone, G. *et al.* Electron localization following attosecond molecular photoionization. *Nature* **465**, 763–6 (2010).

- [7] Kraus, P. M. *et al.* Measurement and laser control of attosecond charge migration in ionized iodoacetylene. *Science (New York, N.Y.)* **350**, 790–795 (2015).
- [8] Stockman, M. I., Kling, M. F., Kleineberg, U. & Krausz, F. Attosecond nanoplasmonic-field microscope. *Nature Photonics* **1**, 539–544 (2007).
- [9] Lewenstein, M., Balcou, P., Ivanov, M. Y., L’Huillier, A. & Corkum, P. B. Theory of high-harmonic generation by low-frequency laser fields. *Physical Review A* **49**, 2117–2132 (1994).
- [10] Shiner, A. D. *et al.* Wavelength Scaling of High Harmonic Generation Efficiency. *Physical Review Letters* **103**, 073902 (2009).
- [11] Barletta, W. *et al.* Free electron lasers: Present status and future challenges. *Nuclear Instruments and Methods in Physics Research Section A: Accelerators, Spectrometers, Detectors and Associated Equipment* **618**, 69–96 (2010).
- [12] Lutman, A. A. *et al.* Experimental Demonstration of Femtosecond Two-Color X-Ray Free-Electron Lasers. *Physical Review Letters* **110**, 134801 (2013).
- [13] Emma, C. *et al.* Experimental demonstration of fresh bunch self-seeding in an X-ray free electron laser. *Applied Physics Letters* **110** (2017).
- [14] Serkez, S. *et al.* Overview of options for generating high-brightness attosecond x-ray pulses at free-electron lasers and applications at the European XFEL. *Journal of Optics* **20**, 024005 (2018).
- [15] Huang, S. *et al.* Generating Single-Spike Hard X-Ray Pulses with Nonlinear Bunch Compression in Free-Electron Lasers. *Physical Review Letters* **119**, 154801 (2017).
- [16] Lutman, A. A. *et al.* Fresh-slice multicolour X-ray free-electron lasers. *Nature Photonics* **10**, 745–750 (2016).
- [17] Emma, P. *et al.* Femtosecond and Subfemtosecond X-Ray Pulses from a Self-Amplified Spontaneous-Emission-Based Free-Electron Laser. *Physical Review Letters* **92**, 074801 (2004).
- [18] Duris, J. *et al.* Tunable isolated attosecond X-ray pulses with gigawatt peak power from a free-electron laser. *Nature Photonics* **14**, 30–36 (2020).
- [19] Hartmann, N. *et al.* Attosecond time–energy structure of X-ray free-electron laser pulses. *Nature Photonics* **12**, 215–220 (2018).
- [20] Guo, Z. *et al.* Experimental demonstration of attosecond pump–probe spectroscopy with an x-ray free-electron laser. *Nature Photonics* (2024).

- [21] Franz, P. *et al.* Terawatt-scale attosecond X-ray pulses from a cascaded superradiant free-electron laser. *Nature Photonics* (2024).
- [22] Young, L. *et al.* Roadmap of ultrafast x-ray atomic and molecular physics. *Journal of Physics B: Atomic, Molecular and Optical Physics* **51**, 032003 (2018).
- [23] Li, S. *et al.* Attosecond coherent electron motion in Auger-Meitner decay. *Science* **375**, 285–290 (2022).
- [24] Li, S. *et al.* Attosecond-pump attosecond-probe x-ray spectroscopy of liquid water. *Science* **383**, 1118–1122 (2024).
- [25] Eichmann, U. *et al.* Photon-recoil imaging: Expanding the view of nonlinear x-ray physics. *Science* **369**, 1630–1633 (2020).
- [26] Alexander, O. *et al.* Attosecond impulsive stimulated X-ray Raman scattering in liquid water. *Science Advances* **10**, eadp0841 (2024).
- [27] Thibault, P. *et al.* High-resolution scanning x-ray diffraction microscopy. *Science* **321**, 379–382 (2008).
- [28] Ho, P. J. *et al.* The role of transient resonances for ultra-fast imaging of single sucrose nanoclusters. *Nature Communications* **11**, 167 (2020).
- [29] Helml, W. *et al.* Ultrashort Free-Electron Laser X-ray Pulses. *Applied Sciences* **7**, 915 (2017).
- [30] Milton, S. V. *et al.* Exponential gain and saturation of a self-amplified spontaneous emission free-electron laser. *Science (New York, N.Y.)* **292**, 2037–2041 (2001).
- [31] Sanchez-Gonzalez, A. *et al.* Accurate prediction of X-ray pulse properties from a free-electron laser using machine learning. *Nature Communications* **8**, 15461 (2017).
- [32] Li, K. *et al.* Prediction on X-ray output of free electron laser based on artificial neural networks. *Nature Communications* *2023 14:1* **14**, 1–9 (2023).
- [33] Alaa El-Din, K. K. *et al.* Efficient prediction of attosecond two-colour pulses from an X-ray free-electron laser with machine learning. *Scientific Reports* *2024 14:1* **14**, 1–10 (2024).
- [34] Decking, W. *et al.* A MHz-repetition-rate hard X-ray free-electron laser driven by a superconducting linear accelerator. *Nature Photonics* **14**, 391–397 (2020).
- [35] Li, S. *et al.* Characterizing isolated attosecond pulses with angular streaking. *Optics Express* **26**, 4531 (2018).

- [36] Heider, R. *et al.* Megahertz-compatible angular streaking with few-femtosecond resolution at x-ray free-electron lasers. *Physical Review A* **100**, 053420 (2019).
- [37] Dingel, K. *et al.* Artificial intelligence for online characterization of ultrashort X-ray free-electron laser pulses. *Scientific Reports* **12**, 17809 (2022).
- [38] Sorokin, A. A. *et al.* Photoelectric Effect at Ultrahigh Intensities. *Physical Review Letters* **99**, 213002 (2007).
- [39] Young, L. *et al.* Femtosecond electronic response of atoms to ultra-intense X-rays. *Nature* **466**, 56–61 (2010).
- [40] Rudek, B. *et al.* Ultra-efficient ionization of heavy atoms by intense X-ray free-electron laser pulses. *Nature Photonics* **6**, 858–865 (2012).
- [41] Rudenko, A. *et al.* Femtosecond response of polyatomic molecules to ultra-intense hard X-rays. *Nature* **546**, 129–132 (2017).
- [42] Mazza, T. *et al.* Mapping Resonance Structures in Transient Core-Ionized Atoms. *Physical Review X* **10**, 041056 (2020).
- [43] Boll, R. *et al.* X-ray multiphoton-induced Coulomb explosion images complex single molecules. *Nature Physics* **18**, 423–428 (2022).
- [44] Guetg, M. W., Lutman, A. A., Ding, Y., Maxwell, T. J. & Huang, Z. Dispersion-Based Fresh-Slice Scheme for Free-Electron Lasers. *Physical Review Letters* **120**, 264802 (2018).
- [45] Gerasimova, N. *et al.* The soft X-ray monochromator at the SASE3 beamline of the European XFEL: from design to operation. *Journal of Synchrotron Radiation* **29**, 1299–1308 (2022).
- [46] Rivas, D. E. *et al.* High-temporal-resolution X-ray spectroscopy with free-electron and optical lasers. *Optica* **9**, 429–430 (2022).
- [47] Grychtol, P. *et al.* Timing and X-ray pulse characterization at the Small Quantum Systems instrument of the European X-ray Free Electron Laser. *Optics Express* **29**, 37429–37442 (2021).
- [48] Li, S. *et al.* “Beam à la carte”: laser heater shaping for attosecond pulses in a multiplexed x-ray free-electron laser (2024). URL <http://arxiv.org/abs/2404.02299>.
- [49] Schmidt, V. *Electron Spectrometry of Atoms using Synchrotron Radiation* Cambridge Monographs on Atomic, Molecular and Chemical Physics (Cambridge University Press, Cambridge, 1997).

- [50] Brunner, C. *et al.* Deep learning in attosecond metrology. *Optics Express*, Vol. 30, Issue 9, pp. 15669-15684 **30**, 15669–15684 (2022).
- [51] Meng, L. *et al.* Deep learning for isolated attosecond pulse reconstruction with the all-optical method. *JOSA B*, Vol. 40, Issue 10, pp. 2536-2545 **40**, 2536–2545 (2023).
- [52] Gal, Y. & Ghahramani, Z. Balcan, M. F. & Weinberger, K. Q. (eds) *Dropout as a bayesian approximation: Representing model uncertainty in deep learning.* (eds Balcan, M. F. & Weinberger, K. Q.) *Proceedings of The 33rd International Conference on Machine Learning*, Vol. 48 of *Proceedings of Machine Learning Research*, 1050–1059 (PMLR, 2016). URL <https://proceedings.mlr.press/v48/gall16.html>.
- [53] Dingel, K. in *Actively controlling and redesigning experiments using the application case of free-electron laser pulse characterization* (eds Tomforde, S. & Krupitzer, C.) *Organic Computing – Doctoral Dissertation Colloquium 2021* 86–98 (kassel university press, 2022).
- [54] Haynes, D. C. *et al.* Clocking Auger electrons. *Nature Physics* 1–7 (2021).
- [55] Mazza, T. *et al.* Resonant Raman Auger spectroscopy on transient core-excited Ne ions. *Journal of Physics B: Atomic, Molecular and Optical Physics* (2024).
- [56] Inhester, L., Hanasaki, K., Hao, Y., Son, S.-K. & Santra, R. X-ray multiphoton ionization dynamics of a water molecule irradiated by an x-ray free-electron laser pulse. *Phys. Rev. A* **94**, 023422 (2016).
- [57] Bhalla, C. P., Folland, N. O. & Hein, M. A. Theoretical *K*-Shell Auger Rates, Transition Energies, and Fluorescence Yields for Multiply Ionized Neon. *Phys. Rev. A* **8**, 649–657 (1973).
- [58] Gryzlova, E. V., Kiselev, M. D., Popova, M. M. & Grum-Grzhimailo, A. N. Evolution of the ionic polarization in multiple sequential ionization: General equations and an illustrative example. *Phys. Rev. A* **107**, 013111 (2023).
- [59] Hoener, M. *et al.* Ultraintense X-ray induced ionization, dissociation, and frustrated absorption in molecular nitrogen. *Physical Review Letters* **104**, 253002 (2010).